Journal of Vacuum Science and Technology B

RESEARCH ARTICLE | JANUARY 29 2026

Characterizing the stability of poly-ethylene glycol surface coatings as a function of environmental conditions for micropatterning applications

Special Collection: Conference on Electron, Ion and Photon Beam Technology and Nanofabrication (EIPBN2025)

Nadav Jacobsen ; Noa Ben-Asher ; Leeya Engel

J. Vac. Sci. Technol. B 44, 024001 (2026)
https://doi.org/10.1116/6.0004946

JVST B
Journal of Vacuum Science & Technology B

ARTICLE

pubs.aip.org/avs/jvb

Characterizing the stability of poly-ethylene glycol surface coatings as a function of environmental conditions for micropatterning applications

Cite as: J. Vac. Sci. Technol. B 44, 024001 (2026); doi: 10.1116/6.0004946
Submitted: 31 August 2025 · Accepted: 23 December 2025 ·
Published Online: 29 January 2026

Nadav Jacobsen,[1] Noa Ben-Asher,[1] and Leeya Engel[1,2,a)]

AFFILIATIONS

[1]Faculty of Mechanical Engineering, Technion—Israel Institute of Technology, Haifa 3200003, Israel
[2]Resnick Sustainability Center for Catalysis, Technion—Israel Institute of Technology, Haifa 3200003, Israel

Note: This paper is part of the Special Topic on the 68th International Conference on Electron, Ion and Photon Beam Technology and Nanofabrication (EIPBN 2025).

[a)]**Author to whom correspondence should be addressed:** Leeya@technion.ac.il

ABSTRACT

Poly-ethylene glycol (PEG) is widely used as an antifouling coating in biomedical applications, including the micropatterning of cells, but its antifouling properties are known to degrade over time. Here, we systematically characterize the degradation of a methoxy PEG succinimidyl valerate coating on poly-L-lysine (PLL) treated glass surfaces as a function of temperature and humidity over a 10-week period. This PEG functionalization strategy is not as well-characterized as the more established PEG grafted to PLL (PLL-g-PEG) coating, but may offer longer term stability. Using a fluorescence-based method to quantify antifouling efficacy, we found that PEG coatings stored dry at room temperature (25 °C) exhibited the highest loss of function. In contrast, storing PEG-coated surfaces in phosphate-buffered saline at both 4 and 25 °C, or dry at −20 °C, effectively preserved their antifouling properties. We used maskless photolithography to selectively degrade PEG and revealed micro-scale and chemical changes in the PEG coating using fluorescence imaging, mass spectrometry, and atomic force microscopy. Our findings provide practical guidelines for optimal shipping and storing conditions for PEG-coated substrates.

I. INTRODUCTION

Poly-ethylene glycol (PEG) is a hydrophilic, inert, high molecular weight molecule, commonly used in pharmaceutical applications such as colonic lavage systems due to its inert properties.[1] It is also used in drug delivery systems where it acts as a solubilizer, stabilizer, taste-masking agent, release-modifier, bioavailability enhancer, carrier for drug payload, or to provide mechanical support.[2,3] One important application is its use as a protein-resistant coating, which is built on foundational work with self-assembled monolayers (SAMs). Prime and Whitesides introduced the use of PEG as an antifouling agent,[4] based on their work on the theory described in Jeon *et al.*[5] and Chen *et al.*[6] When oligo(ethylene oxide) chains, a short-chain version of PEG, are end-attached to gold surfaces, they create coatings that resist nonspecific protein adsorption. The authors systematically varied both PEG chain length and surface density to uncover the key factors governing this resistance, showing that once the PEG occupies a critical mole fraction on the surface, protein adsorption falls to zero. Importantly, they found that longer PEG chains require a lower surface density to achieve the same level of protection.

This foundational understanding of PEG's antifouling behavior paved the way for its use in controlling the spatial arrangement of biological materials. PEG can be patterned on cell culture surfaces to create regions of a substrate that are adhesive or repulsive to cells so that cell shape and distribution on the surface can be controlled.[7–10]

PEG coating has one significant setback; it tends to degrade and lose its antifouling property over time.[11] This primary challenge to its stability stems from its hygroscopic nature, causing it to

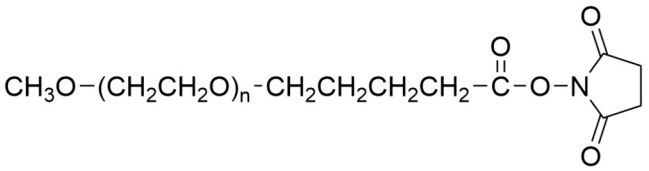

FIG. 1. Chemical structure of methoxy poly-ethylene glycol succinimidyl valerate (mPEG-SVA).

interact strongly with ambient moisture. For example, Baird *et al.*[12] studied how different molecular weights of PEG absorb moisture from the air and undergoes deliquescence. They tested how this process was affected by temperature and by mixing PEG with other common drug ingredients, such as acetaminophen. In another example, the study by Dönmez *et al.*[13] investigates how the refractive index and thickness of thin PEG films change in response to humidity. The researchers found that as humidity increases, the PEG film swells and its optical properties change, undergoing a distinct phase transition from a semi-crystalline to a gel state at around 80% relative humidity. These significant, humidity-induced physical transformations raise critical questions about the integrity and longevity of the chemical surface attachment. Antifouling coatings based on chemicals such as poly(2-methyl-2-oxazoline) (PMOXA), poly(2-methacryloyloxyethyl phosphorylcholine) (PMPC), poly(sulfobetaine methacrylate) (PSBMA) are currently being explored as more stable alternatives to PEG, but these are not commonly used in photolithography based micropatterning.[14,15]

Early cell micropatterning studies functionalized surfaces with PEG via gold-thiol attachment, however over the past decade it has become increasingly common in micropatterning protocols to attach PEG via poly-L-lysine (PLL) to coat glass surfaces instead.[16] PLL-g-PEG brush architectures have been well characterized[17–19] and are stable of the order of hours to several days[15,20] (Fig. S1, supplementary material). Protocols for maskless photopatterning that employ a longer lasting, two-step PEG functionalization method using methoxy PEG (mPEG) coupled with a succinimidyl valerate (SVA) ester that can covalently bond to PLL have been reported to be stable for up to a month when kept dry at 4 °C[20] (Fig. 1). While it may offer longer term stability, this PEG-PLL coating has not yet been well characterized in a micropatterning context. Therefore, here we aimed to characterize the rate of degradation of mPEG-SVA attached to glass surfaces via covalent bonds to PLL as a function of humidity and temperature and following maskless photopatterning. The results of this study inform optimal storage and shipping conditions for PEG-treated and micropatterned surfaces as well as improve experimental micropatterning workflows.

II. METHODS

We functionalized glass coverslips with PEG following established methods[21] and then either selectively degraded the coating through maskless lithography or allowed the coating to degrade over time under different storage conditions (Fig. 2).

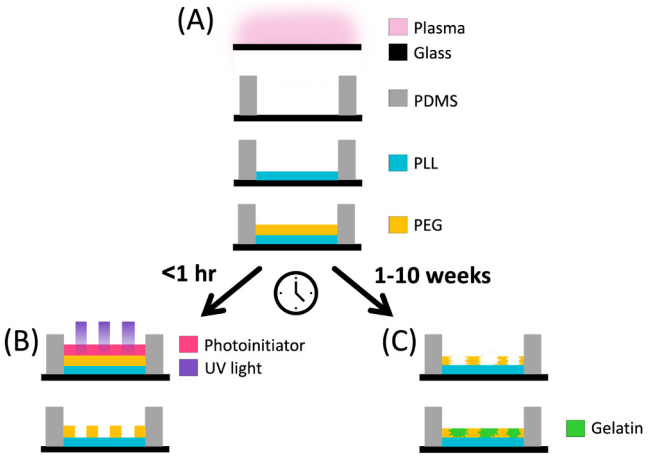

FIG. 2. Schematic of experimental workflow for preparing and testing PEG-functionalized surfaces. (a) The process begins with the layer-by-layer assembly of a functional surface on a plasma-treated glass coverslip, onto which a PDMS sticker is applied to create controlled wells. A foundational layer of poly-L-lysine (PLL) is deposited, followed by a covalently attached passivating layer of poly-ethylene glycol (PEG). This surface is then subjected to two distinct degradation protocols. (b) Spatially controlled degradation via maskless photolithography. A photoinitiator (pink) is applied to the PEG layer, and UV light exposure (purple) is used to create precise micropatterns. (c) A time-dependent environmental degradation assay. Samples are incubated for extended periods (up to 10 weeks) under various conditions. The extent of PEG layer degradation is then quantified by the amount of fluorescently labeled gelatin that can bind to the exposed regions of the substrate.

A. PEG surface functionalization

Glass coverslips (epredia, rectangular coverglass, size 24 × 60 mm #1.5) were treated in a plasma etcher (Plasma Etch P-50) for one minute using atmospheric plasma. Immediately after plasma exposure, rectangular silicone stickers, 0.254 mm thick, each containing three holes with a diameter of 5 mm, were applied to the coverslips to create wells (Fig. 3). Each well was then

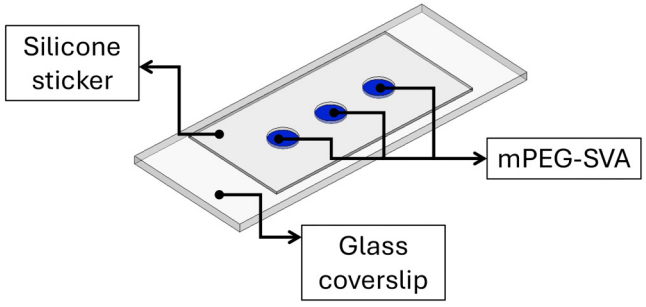

FIG. 3. Schematic of the experimental setup, showing a #1.5 glass coverslip with a silicone stencil. The wells formed by the stencil are coated with polyethylene glycol.

promptly filled with 28 μl of a 0.01% poly-L-lysine (PLL) solution (Sigma-Aldrich, P4707, 0.1 mg/ml, $MW = 70-150$ kDa). This procedure was replicated for all coverslips. The samples were then placed in Petri dishes and left to incubate overnight in a refrigerator at 4 °C.

The following day, the samples were removed from the refrigerator and washed with a phosphate-buffered saline (PBS) solution (Sigma-Aldrich, D8537). For the washing procedure, each coverslip was held by its edge while PBS was dispensed onto the upper surface using a pipet or a squeeze bottle, ensuring that the solution flushed all three wells.

Following the rinse, the PEG-SVA (Laysan Bio) solution was prepared. The required amount was retrieved from the −20 °C freezer and allowed to thaw at room temperature for 10 min to prevent moisture condensation. The PEG-SVA powder ($MW = 5$ kDa) was then dissolved in a 0.1M HEPES buffer solution (*p*H 8.5) (Sigma-Aldrich, H3537) to a final concentration of 100 mg/ml. A volume of 28 μl of the resulting PEG solution was applied to each well, after ensuring excess PBS from the washing step was removed. The samples were incubated for 1 h to allow for the covalent attachment of PEG to the surface. Finally, the samples were washed again with PBS to remove excess PEG that was not attached to the surface (Figs. 2 and S2, supplementary material).

B. Validation of surface functionalization

Time-of-flight secondary ion mass spectrometry (TOF-SIMS) was employed to provide direct, stage-by-stage chemical validation of the surface functionalization, from the foundational adhesion layer to the final patterned architecture. Three stages were assessed: bare glass, which was used as a control, glass coated with PLL, and fully functionalized glass coated with PLL followed by PEG. SIMS spectroscopy was performed using the TOF.SIMS 5 (IONTOF GmbH).

C. Degradation assessment

To test the time scales over which passive degradation occurs, we divided our samples into different storage conditions. We chose three temperatures that are accessible to most laboratories: freezer (−20 °C), refrigerator (4 °C), and room temperature (25 °C). We stored the samples either in PBS or air (with 52%*RH*). For the latter condition, we rinsed off the PBS with distilled water to prevent salt crystallization during air drying. We performed three independent experiments. Each experiment was conducted over a 10-week period, with measurements taken at one-week intervals, totaling 10 data points per condition. For each data point, we acquired two to three images from distinct regions within each well (two images per well in the first experiment, and three images per well in the subsequent two experiments), yielding a total of six to nine images per sample per week to ensure data robustness.

As a control, we measured one sample on the same day of the PEG coating (week 0). In each following measurement, we rinsed the samples to be tested with PBS and incubated them for 1 h in 0.1 mg/ml solution of pig gelatin fluorescently tagged with Oregon Green 488 in PBS (Thermo-Fisher Scientific, G13186). We prepared an additional control surface each time we performed microscopy—one coverslip that was treated with plasma and incubated with the green tagged gelatin. This was done to get the theoretical maximum value of attached gelatin. Prior to imaging, we filled each well with PBS to rehydrate the PEG so that it is in the extended conformation.[22,23]

We acquired fluorescent images using either an Olympus IX83 inverted microscope with a 20× air objective or a Nikon ECLIPSE Ti2-E spinning disk microscope using a 20× air objective.

Using fluorescence microscopy, we measured the mean illumination intensity of the green tagged gelatin in each sample, taking several measurements from each well.[24] We then normalized this value to a control sample, not treated with PEG so that it had the highest mean value (Fig. S3, supplementary material). Taking into account that the signal is from the gelatin that adhered to regions where the PEG coating is compromised, we describe the quality of PEG coating by taking the complement to one of the normalized values. This way we get a measure of the antifouling efficacy. The resulting calculation is as follows:

$$\text{Antifouling Efficacy} = 1 - \frac{\text{mean illumination}}{\text{max illumination}}. \tag{1}$$

To characterize the general trend of degradation over time, we used a smoothing function to analyze our data. We chose the LOWESS algorithm, which averages all the points within a window that surrounds a point, which we chose to be 75% of the data, while giving weights to each point depending on the distance from the point of interest $d \in [-1, 1]$,[25]

$$w_i = (1 - |d|^3)^3. \tag{2}$$

To get statistically robust results, we conducted three independent repetitions of the experiment and took the average of the final results from each repetition. To calculate the pooled standard deviation (SD), we used the known formulation

$$s_p = \sqrt{\frac{\sum_{i=1}^{k} (n_i - 1)s_i^2}{\sum_{i=1}^{k} (n_i - 1)}}, \tag{3}$$

where s_p is the pooled SD, k is the total number of groups being pooled (3, in our case), n_i is the size of the ith sample, and s_i is the SD of the ith group.

We conducted T-tests on the combined data from the three iterations with a two-sample T-test comparing no degradation from week 0 against week 10 degradation, checking the next set of hypotheses,

H_0: mean(Week 0) = mean(Week 10) (no degradation).
H_1: mean(Week 0) > mean(Week 10) (significant degradation).

D. Micropatterning using maskless lithography

To better understand the topography of PEG coatings, we selectively degraded the PEG surface in a pattern of repeating lines and performed measurements using an atomic force microscope (AFM).[21] After applying the PEG coating as previously, we applied

a thin layer of photoinitiator, 4-benzoylbenzyl-trimethylammonium chloride (PLPP, Alveole), diluted 1:6 in ethanol 97%. When the PLPP is exposed to UV light, it becomes acidic and cleaves the PEG.[26] Micropatterning was performed using the Alvéole PRIMO maskless photopatterning system (Alvéole, Paris, France).[20] We then use the PRIMO system to pattern the surface using UV light that is directed via a micromirror array. After patterning, we wash off remaining PLPP using PBS. We are then left with the patterned PEG surface. The pattern we chose consists of repeating lines with a width of 2 μm with a 5 μm space between them [Fig. 9(a), left image]. This repeating pattern allowed us to measure the height difference between the PEG and the degraded regions, regardless of where the AFM tip landed on the sample.

UV exposure dosages used for patterning were in the range of 15−50 mJ/mm^2.

Atomic force microscope (AFM) measurements were performed using a Cypher ES Environmental AFM (Asylum Research, Oxford Instruments). Topography images were acquired in a tapping mode using an AC240 probe (first resonance frequency ~70 kHz, spring constant ~2.0 N/m).

Fluorescent images for this method were taken using a Nikon ECLIPSE Ti2-E spinning disk microscope using a 20× air objective.

III. RESULTS AND DISCUSSION

A. PEG distribution is altered by photopatterning

We used TOF-SIMS to determine the surface composition of our samples. We began with a control substrate, a bare glass coverslip, to establish a chemical baseline. The glass coverslip produced a spectrum dominated by inorganic constituents characteristic of glass, with intense peaks corresponding to Na^+, K^+, and Si^+/SiO^+. This spectrum showed only minor hydrocarbon fragments, attributed to typical ambient surface contamination.

In stark contrast, the spectrum for PLL-coated glass confirmed the successful deposition of the poly-L-lysine (PLL) adhesion layer through the appearance of intense nitrogen-containing organic fragments. The most prominent characteristic peaks observed for the PLL coating included strong signals for $C_4H_{11}N^+$ (m/z 73), $C_5H_{12}N^+$ (m/z 86), and $C_3H_8N^+$ (m/z 58), all derived from the lysine structure (Fig. 4).

Analysis of PEG-coated glass provided direct chemical evidence for the PEG attachment. The most significant observation in its mass spectrum was the appearance of a strong peak at m/z 45, unequivocally assigned to the ethoxy fragment ($C_2H_5O^+$), the primary and widely accepted marker for PEG. This finding was further supported by the observation of another oxygen-containing fragment, CH_3O^+, at m/z 31, which is consistent with the fragmentation of the terminal methoxy group of the mPEG-SVA molecule used in our study. Critically, characteristic PLL-related amine fragments, most notably $C_4H_{11}N^+$ at m/z 73, were still clearly detectable (Fig. 5).

TOF-SIMS imaging was also used to validate the successful spatial micropatterning of the PEG layer. 2D chemical maps were acquired simultaneously for multiple ions over a 500 × 500 μm^2 and 100 × 100 μm^2 areas. The results showed a clear and distinct periodic pattern exclusively in the ion map corresponding to the

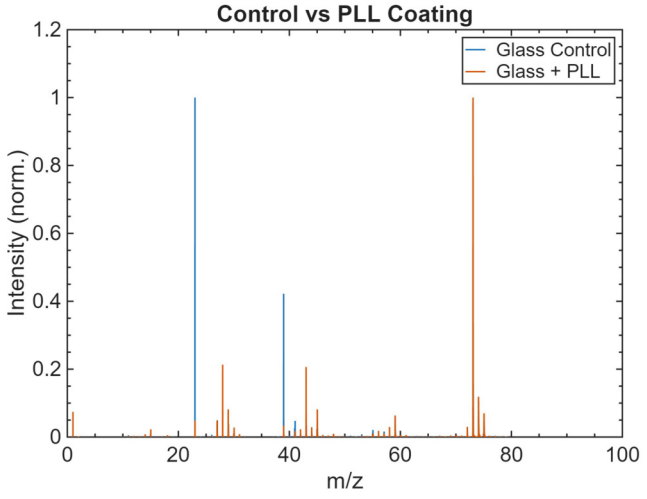

FIG. 4. Comparison of normalized positive ion ToF-SIMS intensities for bare glass control (blue) and PLL-coated glass (orange). The bare glass spectrum is dominated by inorganic substrate ions, specifically Na^+ (m/z 23) and K^+ (m/z 39/41). The deposition of the Poly-L-lysine (PLL) layer suppresses these substrate signals and results in the appearance of characteristic nitrogen-containing organic fragments, most notably the aliphatic ammonium fragment $C_4H_{11}N^+$ at m/z 73.

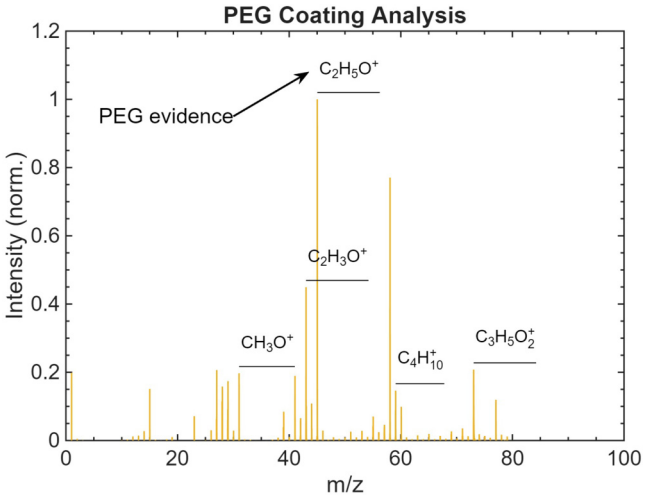

FIG. 5. Normalized positive ion ToF-SIMS spectrum acquired from the PEG-coated glass sample. The analysis reveals a distinct chemical signature dominated by the peak at m/z 45, corresponding to the ethoxy fragment $C_2H_5O^+$, which is identified as the principal diagnostic marker for the PEG coating. Additional oxygen-containing fragments characteristic of PEG fragmentation are observed, including CH_3O^+ (m/z 31) and $C_2H_3O^+$. Nonspecific hydrocarbon fragments such as $C_4H_{10}^+$ (m/z 58) are also present. The high intensity of the $C_2H_5O^+$ signal confirms the successful formation of a PEG overlayer on the PLL-modified surface.

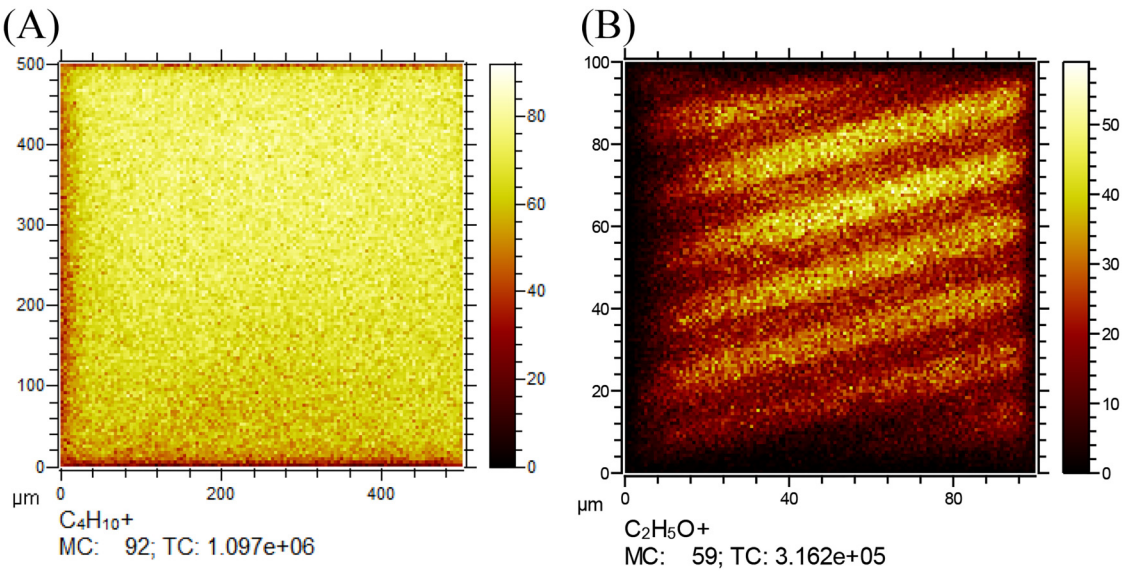

FIG. 6. 2D TOF-SIMS chemical imaging of patterned PEG-coated glass. (a) Ion map of the nonspecific hydrocarbon fragment $C_4H_{10}^+$ (m/z 58) acquired over a 500 × 500 μm^2 area, displaying a homogeneous distribution typical of background organic contamination. (b) Corresponding ion map acquired over (100 × 100 μm^2) area of the PEG-specific ethoxy fragment $C_2H_5O^+$ (m/z 45) from the same region. A distinct periodic pattern is clearly resolved, confirming the spatial selectivity of the PEG coating.

PEG-specific ethoxy fragment ($C_2H_5O^+$). This spatial pattern was entirely absent in the maps for ubiquitous ions (H^+), substrate-derived ions (Si^+), and the nonspecific hydrocarbon fragment $C_4H_{10}^+$ (Fig. 6).

In summary, the TOF-SIMS analysis provided a comprehensive validation of both the sequential chemical layering and the precise spatial patterning, establishing a strong and reliable foundation for the subsequent topographical and functional characterizations.

B. Antifouling efficacy of PEG varies as a function of storage conditions

Samples stored in air at room temperature (25 °C) or in the refrigerator (4 °C) significantly degraded after 10 weeks of storage with those stored at 4 °C experiencing less degradation relative to samples stored at 25 °C (Fig. 7). Samples that were stored dry in the freezer (−20 °C) were protected from degradation over the duration of the experiment. Storage in PBS protected the antifouling properties of the PEG at room temperature and in the refrigerator compared to samples kept at the same temperatures that were dried prior to storage (Fig. 8). We conclude that PEG-based antifouling coatings prepared by adsorbing PLL on glass followed by coupling with mPEG-SVA in PBS or dry in a freezer appear to be optimal, showing negligible degradation after 10 weeks in storage (Table S1, supplementary material).

Degradation of the antifouling efficacy may be due to several mechanisms, including oxidation of PEG or changes relating to the PLL-glass attachment, which we did not determine here (see Figs. S2 and S7 in the supplementary material). Another limitation of our study is that we did not monitor fluctuations in relative humidity in the laboratory during the storage period, which may have influenced the amount of adsorbed water vapor in the dry-stored samples.

From Figs. 8(a)–8(e), it is evident that the fluorescence data displayed considerable variability, with high standard deviations for several data points. This is due to the nonuniform nature of the spontaneous degradation (Fig. S5, supplementary material).

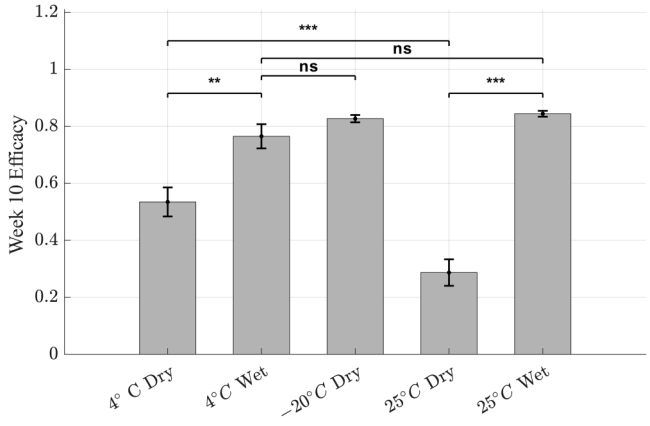

FIG. 7. Antifouling efficacy after 10 weeks of storage under different environmental conditions. Bars represent the mean normalized efficacy, with error bars indicating the standard error of the mean (SEM). Statistical significance between designated pairs was determined using two-sample unpaired Welch's t-tests. [ns: $p \geq 0.05$, (∗): $p < 0.05$, (∗∗): $p < 0.01$, (∗∗∗): $p < 0.001$].

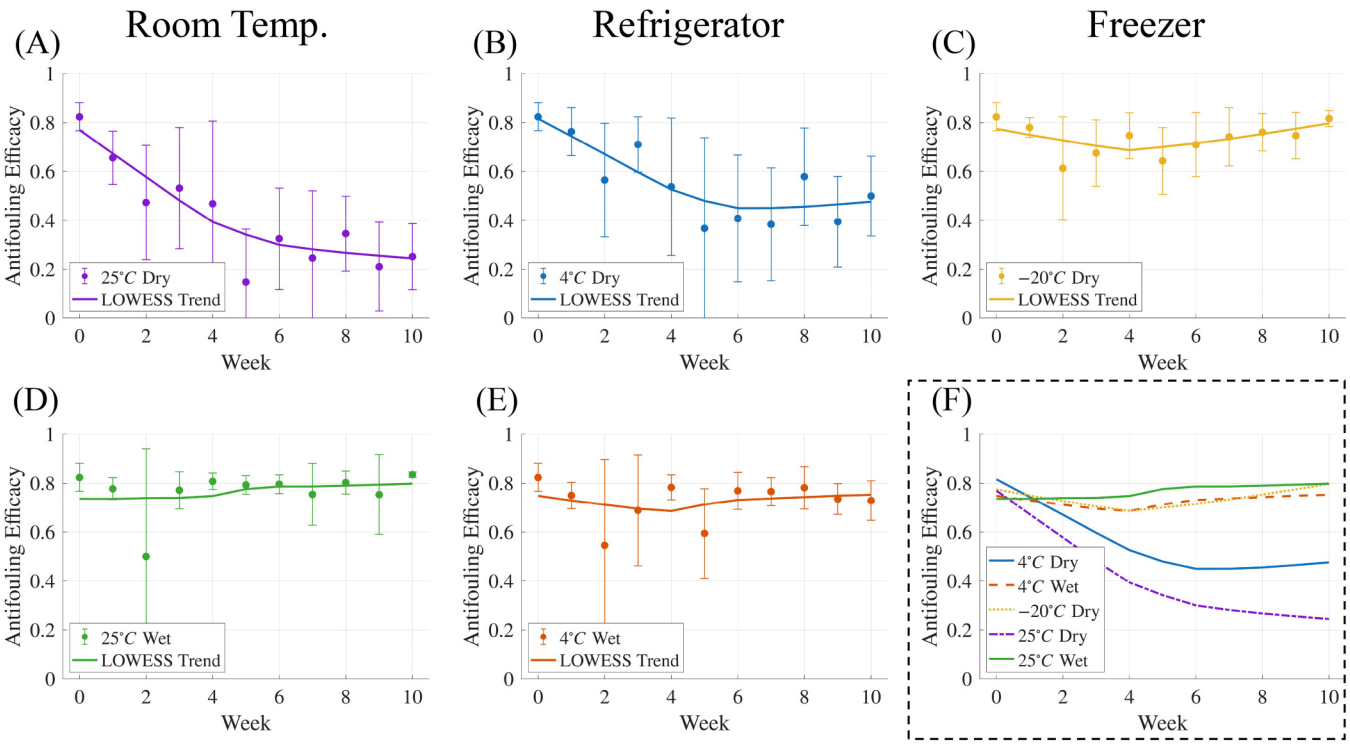

FIG. 8. Long-term stability of antifouling efficacy under various storage conditions. The antifouling efficacy of the coating was evaluated over a 10-week period. (a)–(c) Efficacy of coatings stored dry in air at (a) room temperature (25 °C), (b) in a refrigerator (4 °C), and (c) in a freezer (−20 °C). (d) and (e) Efficacy of coatings stored wet in phosphate-buffered saline (PBS) at (d) room temperature (25 °C) and (e) in a refrigerator (4 °C). In panels (a)–(e), individual points represent the mean efficacy, and error bars represent the standard deviation. The solid line is the Locally estimated scatterplot smoothing (LOESS) trend, while the dashed line indicates the initial efficacy at week 0. (f) A direct comparison of the LOESS trends for the dry and wet storage conditions, demonstrating that storage at −20 °C (dry) and under both wet conditions (in PBS at 4 °C and 25 °C) best preserved the coating's antifouling properties.

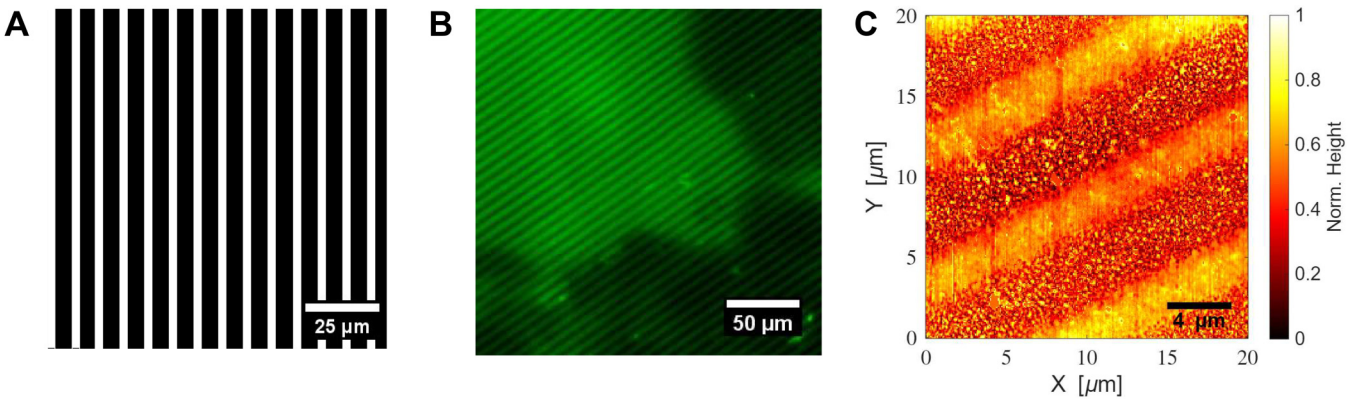

FIG. 9. Pattern transfer from a digital mask to a poly-ethylene glycol (PEG)-coated surface for selective protein attachment. (a) The digital mask (.tif file) with a line pattern used for photopatterning the PEG surface. Scale bar: 25 μm. (b) Fluorescence spinning disk microscopy image confirming the site-specific attachment of fluorescently labeled gelatin along the patterned lines where the PEG was degraded. Scale bar: 50 μm. (c) Atomic Force Microscopy (AFM) image showing the topography of the patterned PEG surface submerged in PBS. Both microscopy images confirm the successful transfer of the pattern from the digital mask to the hydrogel surface. Scale bar: 4 μm.

Several samples not included in the degradation analysis were air dried with small amounts of PBS remaining on the PEG-coated surfaces. Upon rehydration in PBS, fluorescence microscopy of these surfaces revealed an intriguing phenomenon: spontaneous pattern formation. In Fig. S4(b) (supplementary material), dark patches devoid of gelatin can be seen, which ostensibly indicate intact PEG. These patterns may have resulted from salt crystallizing on top of the sample as the PBS solution dried, protecting the PEG from degrading in these regions. In addition, spontaneous patterning was also observed on samples that were kept dry in the freezer, as can be seen in Fig. S4(a) (supplementary material). The mechanism by which these patterns form and whether their geometry can be controlled would be an interesting topic for future research.

C. Photopatterning PEG-coated glass alters surface topography

To validate PEG patterning using maskless lithography and to check the topographical changes induced, we used an AFM to scan the patterned PEG surface alongside fluorescence microscopy of patterned PEG surfaces backfilled with fluorescently tagged gelatin to verify the patterning.

The scans and images confirm successful patterning of the surfaces. Fluorescence microscopy demonstrated good correspondence between the digital mask and protein adhesion patterns. Additionally, AFM scanning revealed notable height differences (~14 nm) between the patterned lines and the unmodified PEG regions (Fig. 9). This height difference is in the same order of magnitude as measured for maskless photopatterned PLL-g-PEG surfaces (~6 nm) and indicates that the PEG coating undergoes structural changes during the UV exposure.[2]

IV. CONCLUSIONS

This study provides a systematic evaluation of the stability of PEG-based antifouling coatings on glass surfaces. Our time-dependent analysis reveals that PEG-coated surfaces should be stored in PBS, as air-exposed samples showed the most pronounced loss of antifouling efficacy. Interestingly, refrigeration alone offered only moderate protection, while freezing at −20 °C substantially preserved functionality with insignificant degradation over 10 weeks. These results underscore the importance of a PBS layer in the storage and use of PEG-functionalized surfaces.

In addition, our AFM and fluorescence-based examination of PEG degradation via maskless lithography demonstrates the successful targeted degradation and consequent patterning of the substrate. While our method of assessing antifouling efficacy using fluorescent gelatin provides useful trends, it is susceptible to measurement noise, highlighting the need for complementary, more direct surface characterization techniques in future work. Nevertheless, our findings inform best practices for preserving PEG coatings and contribute to the optimization of surface patterning strategies in mechanobiology and tissue engineering research.

SUPPLEMENTARY MATERIAL

Supplementary material includes supporting data and figures referenced in the main text. These materials provide additional validation of experimental methods, characterization results, and observed trends: Fig. S1: antifouling degradation trends of PLL-g-PEG coatings over 12 days under different storage conditions; Fig. S2: FTIR spectra comparing glass, PLL-coated, and PEG-functionalized surfaces; Fig. S3: fluorescence micrographs showing gelatin adsorption on various control surfaces; Fig. S4: evidence of spontaneous pattern formation on dried PEG surfaces, suggesting protection by salt crystallization; Fig. S5: examples of nonuniform PEG degradation under various conditions; Fig. S6: fluorescence micrographs showing how UV exposure dosage affects pattern quality; Fig. S7: Raman spectra comparing mPEG-SVA, PLL, and PEG-PLL-coated surfaces; Table S1: results of two-sample *t*-tests comparing antifouling efficacy at week 0 and week 10 for different storage conditions.

ACKNOWLEDGMENTS

This work was supported by the Israel Science Foundation (ISF) Personal Research Grant No. 1925/23. L.E. is a Diane and Guilford Glazer Foundation Faculty Fellow. We acknowledge valuable insights of Shaul Michaelson (Surface Science Characterization Center, Department of Materials Science and Engineering, Technion—IIT, Israel) and thank him for conducting the TOF-SIMS measurements. We thank Karam Yassin from the Nancy and Stephen Grand Technion Energy Program at the Technion—IIT for conducting the AFM measurements in the Hydrogen Technologies Research Laboratory. We thank Eyal Zussman and Rita Vilensky for helpful advice and FTIR measurements. We thank Joshua Grolman and Thekra Msarwe for helpful advice and Raman spectroscopy measurements.

AUTHOR DECLARATIONS

Conflict of Interest

The authors have no conflicts to disclose.

Author Contributions

Nadav Jacobsen: Conceptualization (equal); Data curation (equal); Formal analysis (equal); Investigation (equal); Methodology (equal); Project administration (equal); Resources (equal); Software (equal); Validation (equal); Visualization (equal); Writing – original draft (equal). **Noa Ben-Asher:** Investigation (equal); Methodology (equal); Resources (equal); Writing – review & editing (equal). **Leeya Engel:** Conceptualization (equal); Formal analysis (equal); Funding acquisition (equal); Methodology (equal); Project administration (equal); Supervision (equal); Visualization (equal); Writing – original draft (equal); Writing – review & editing (equal).

DATA AVAILABILITY

The data that support the findings of this study are available from the corresponding author upon reasonable request.

REFERENCES

[1]J. Aronson, "Glycols," in *Meyler's Side Effects of Drugs*, 16th ed. (Elsevier, Oxford, 2016), pp. 567–570.
[2]L. P. Dow *et al.*, Nat. Commun. **13**, 7831 (2022).

[3]A. A. D'souza and R. Shegokar, Expert Opin. Drug Deliv. **13**, 1257 (2016).
[4]K. L. Prime and G. M. Whitesides, J. Am. Chem. Soc. **115**, 10714 (1993).
[5]S. Jeon, J. Lee, J. Andrade, and P. De Gennes, J. Colloid Interface Sci. **142**, 149 (1991).
[6]S. Chen, L. Li, C. Zhao, and J. Zheng, Polymer **51**, 5283 (2010).
[7]M. Mrksich, Curr. Opin. Colloid Interface Sci. **2**, 83 (1997).
[8]R. Singhvi, A. Kumar, G. P. Lopez, G. N. Stephanopoulos, D. I. Wang, G. M. Whitesides, and D. E. Ingber, Science **264**, 696 (1994).
[9]L. Engel, G. Gaietta, L. P. Dow, M. F. Swif, G. Pardon, N. Volkmann, W. I. Weis, D. Hanein, and B. L. Pruitt, J. Micromech. Microeng. **29**, 115018 (2019).
[10]L. Engel, C. G. Vasquez, E. A. Montabana, B. M. Sow, M. P. Walkiewicz, W. I. Weis, and A. R. Dunn, J. Struct. Biol. **213**, 107791 (2021).
[11]W. A. Laftah and W. A. W. A. Rahman, Environ. Sci.: Adv. **4**, 824 (2025).
[12]J. A. Baird, R. Olayo-Valles, C. Rinaldi, and L. S. Taylor, J. Pharm. Sci. **99**, 154 (2010).
[13]G. Dönmez, Y. Yilmaz, S. Irmak, C. J. O'Connor, and H. Zareie, Appl. Phys. A **88**, 757 (2007).
[14]B. Pidhatika, M. Rodenstein, Y. Chen, E. Rakhmatullina, A. Mühlebach, C. Acikgöz, M. Textor, and R. Konradi, Biointerphases **7**, 1 (2012).
[15]Y. Chen, B. Pidhatika, T. von Erlach, R. Konradi, M. Textor, H. Hall, and T. Lühmann, Biointerphases **9**, 031003 (2014).
[16]Y. Wu, J. Lian, V. R. Goncçales, R. Pardehkhorram, W. Tang, R. D. Tilley, and J. J. Gooding, Langmuir **36**, 5243 (2020).
[17]S. Pasche, M. Textor, L. Meagher, N. D. Spencer, and H. J. Griesser, Langmuir **21**, 6508 (2005).
[18]M. Heuberger, T. Drobek, and N. D. Spencer, Biophys. J. **88**, 495 (2005).
[19]S. Tosatti, S. De Paul, A. Askendal, S. VandeVondele, J. Hubbell, P. Tengvall, and M. Textor, Biomaterials **24**, 4949 (2003).
[20]C. Melero, A. Kolmogorova, P. Atherton, B. Derby, A. Reid, K. Jansen, and C. Ballestrem, J. Vis. Exp. **152**, e60092 (2019).
[21]L. Engel, R. Held, C. G. Vasquez, W. I. Weis, A. R. Dunn, "Micropatterning EM grids for cryo-electron tomography of cells," Nature Commun. (published online 2025).
[22]T. Farhan, O. Azzaroni, and W. T. Huck, Soft Matter **1**, 66 (2005).
[23]S. Riechers, Q. Zhong, N.-N. Yin, A. Karsai, S. R. da Rocha, and G.-Y. Liu, J. Drug Deliv. **2015**, 535683.
[24]J. Schindelin *et al.*, Nat. Methods **9**, 676 (2012).
[25]Y. Dai, Y. Wang, M. Leng, X. Yang, and Q. Zhou, Energy **256**, 124661 (2022).
[26]P.-O. Strale, A. Azioune, G. Bugnicourt, Y. Lecomte, M. Chahid, and V. Studer, Adv. Mater. **28**, 2024 (2016).